Electronic Supplementary Material (ESI) for Nanoscale.

Ruthenium single-atom doping-driven modulation of Co_3O_4 spinel tetrahedral site 3d-orbital occupancy in lithium-oxygen batteries

Yining Fan[a,#], Ting Li[a,#], Bin Li [a,#], Anjun Hu[a,b,], Dongfen Li[b], Kun Li[a], Borui Yang[a], Yu Pan[a], Jing Liu[a,]*, Jianping Long[a,]**

[a] College of Materials and Chemistry & Chemical Engineering, Chengdu University of Technology, 1#, Dongsanlu, Erxianqiao, Chengdu 610059, Sichuan, P. R. China

[b] College of Computer Science and Cyber Security, Chengdu University of Technology, 1#, Dongsanlu, Erxianqiao, Chengdu 610059, Sichuan, P. R. China

[#] These authors contributed to this work equally.

*Corresponding author: anjunhu@cdut.edu.cn (Anjun Hu); jingliu@cdut.edu.cn (Jing Liu); longjianping@cdut.cn (Jianping Long)

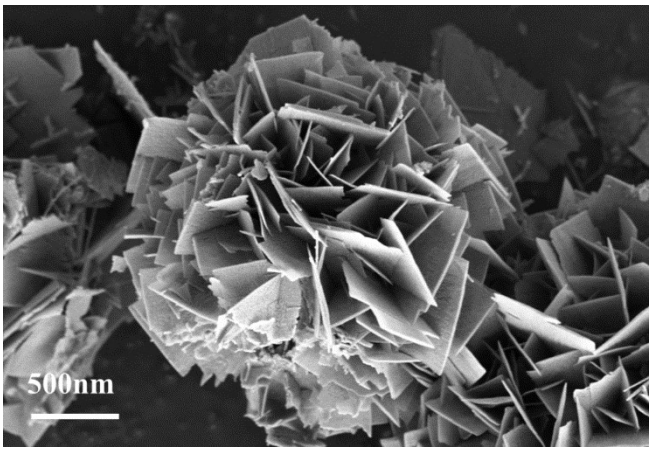

Figure S1. SEM images of the Co_3O_4.

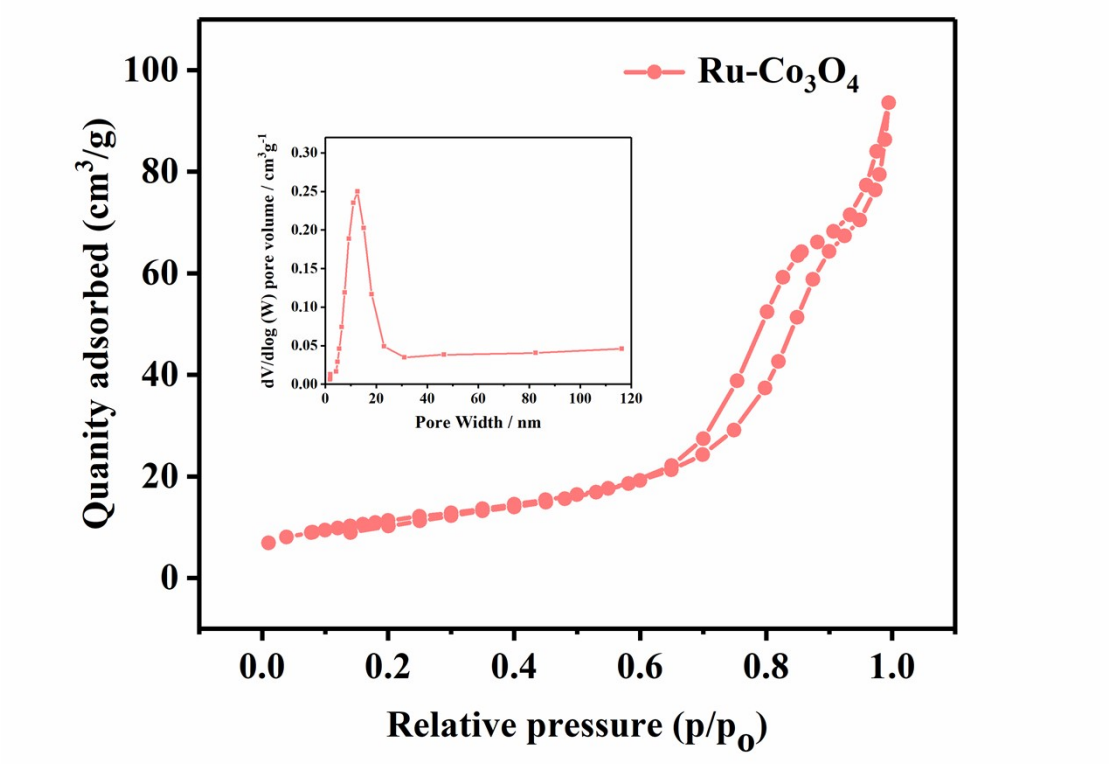

Figure S2. Nitrogen adsorption/desorption isotherms of Ru-Co_3O_4

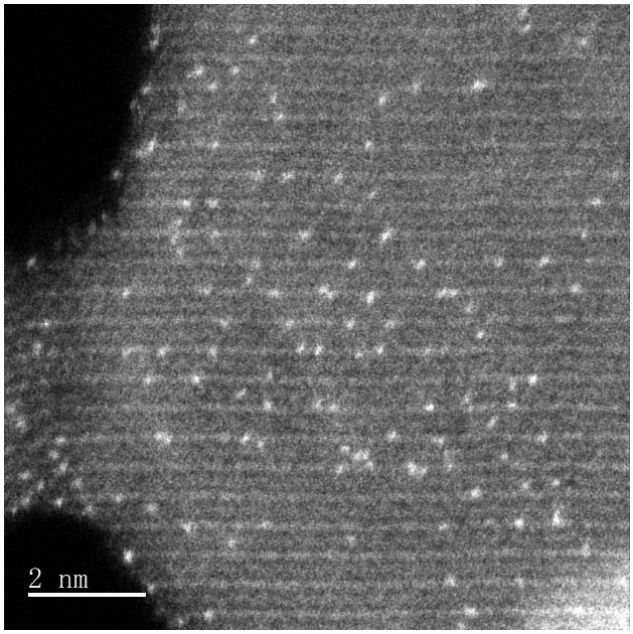

Figure S3. Aberration-corrected HAADF-STEM observation for Ru-Co_3O_4.

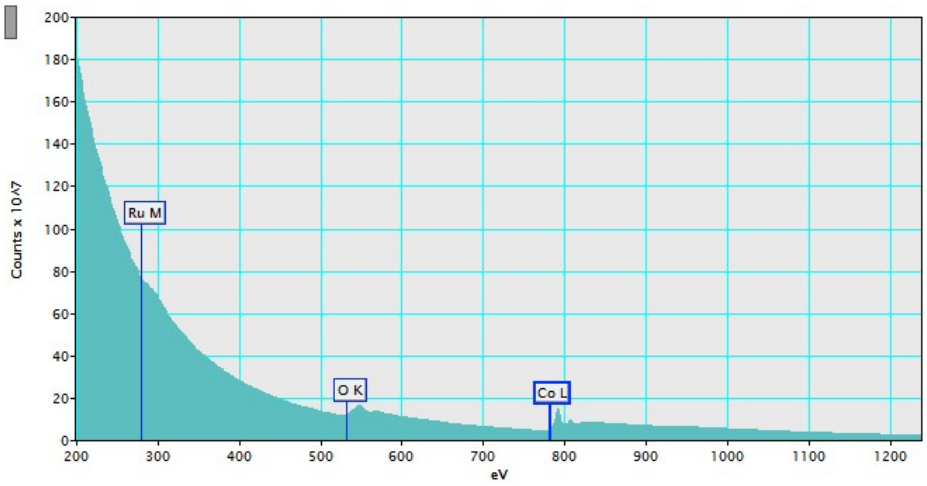

Figure S4. Single-atom EELS spectra extracted from two atomic positions highlighted in bule and yellow in Fig.1g.

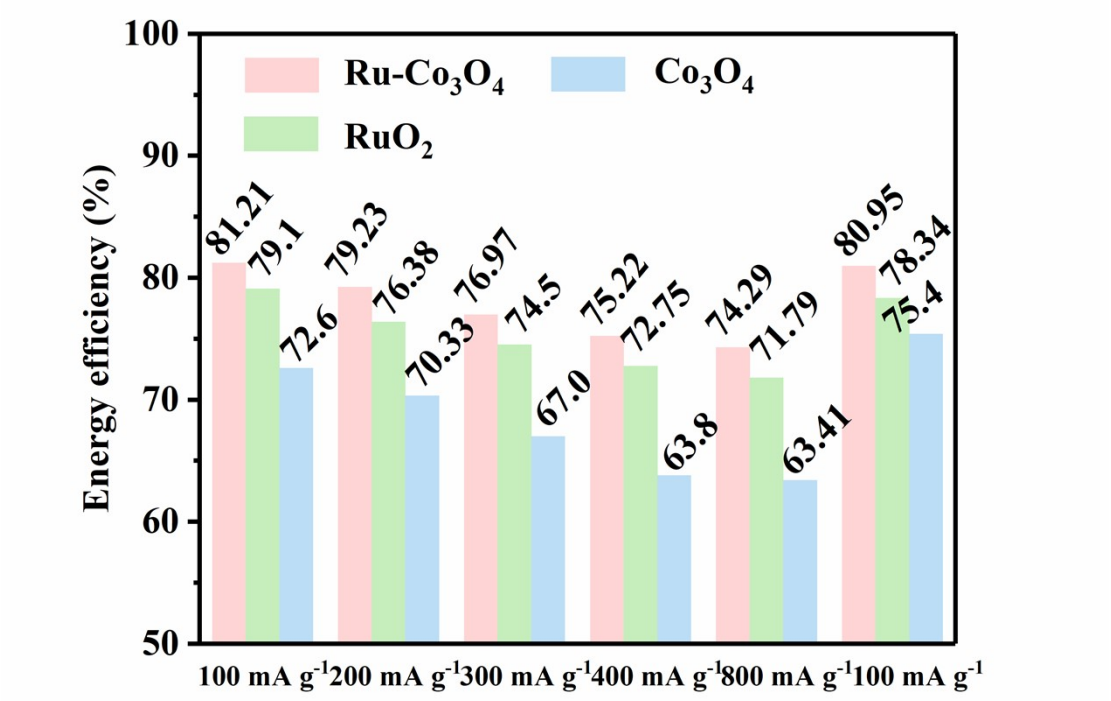

Figure S5. The energy efficiency of Ru-Co_3O_4, RuO_2 and Co_3O_4 at different current density in LOBs.

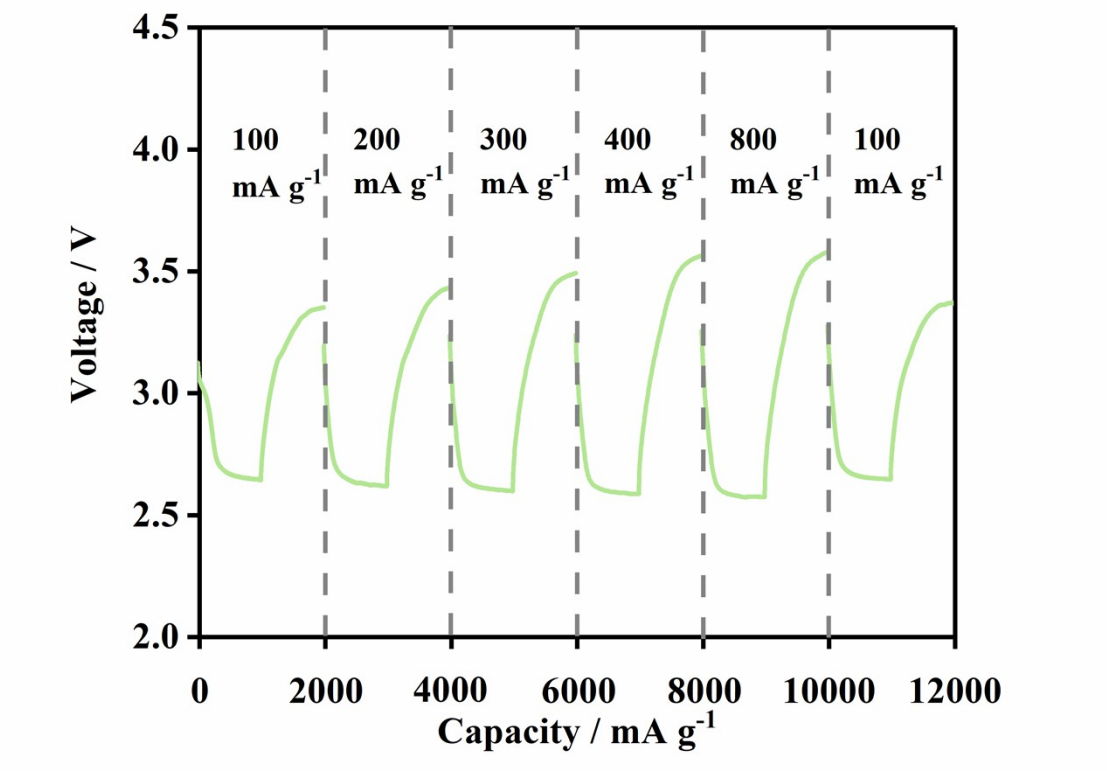

Figure S6. Rate capability of RuO_2 based Li-O_2 batteries.

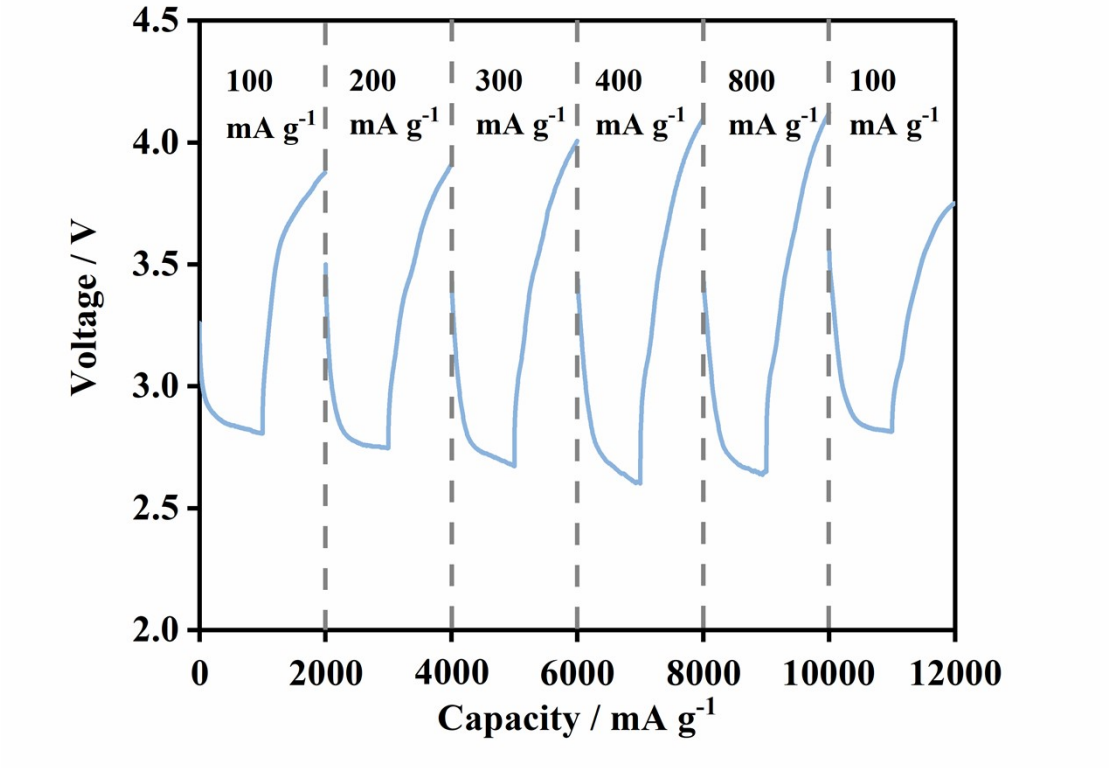

Figure S7. Rate capability of Co_3O_4 based Li-O_2 batteries.

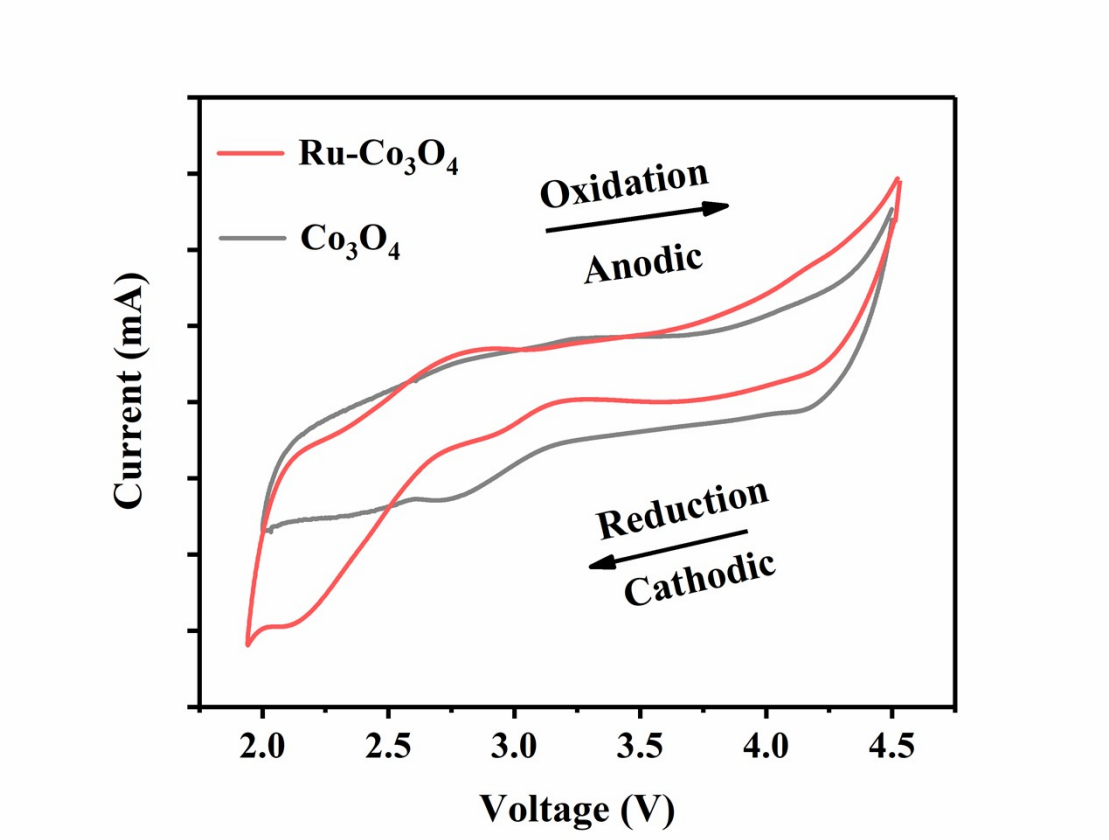

Figure S8. CV curves of Ru-Co_3O_4 and Co_3O_4 under the voltage window of 2.0-4.5 V and the scanning rate of 0.1mV s^{-1}.

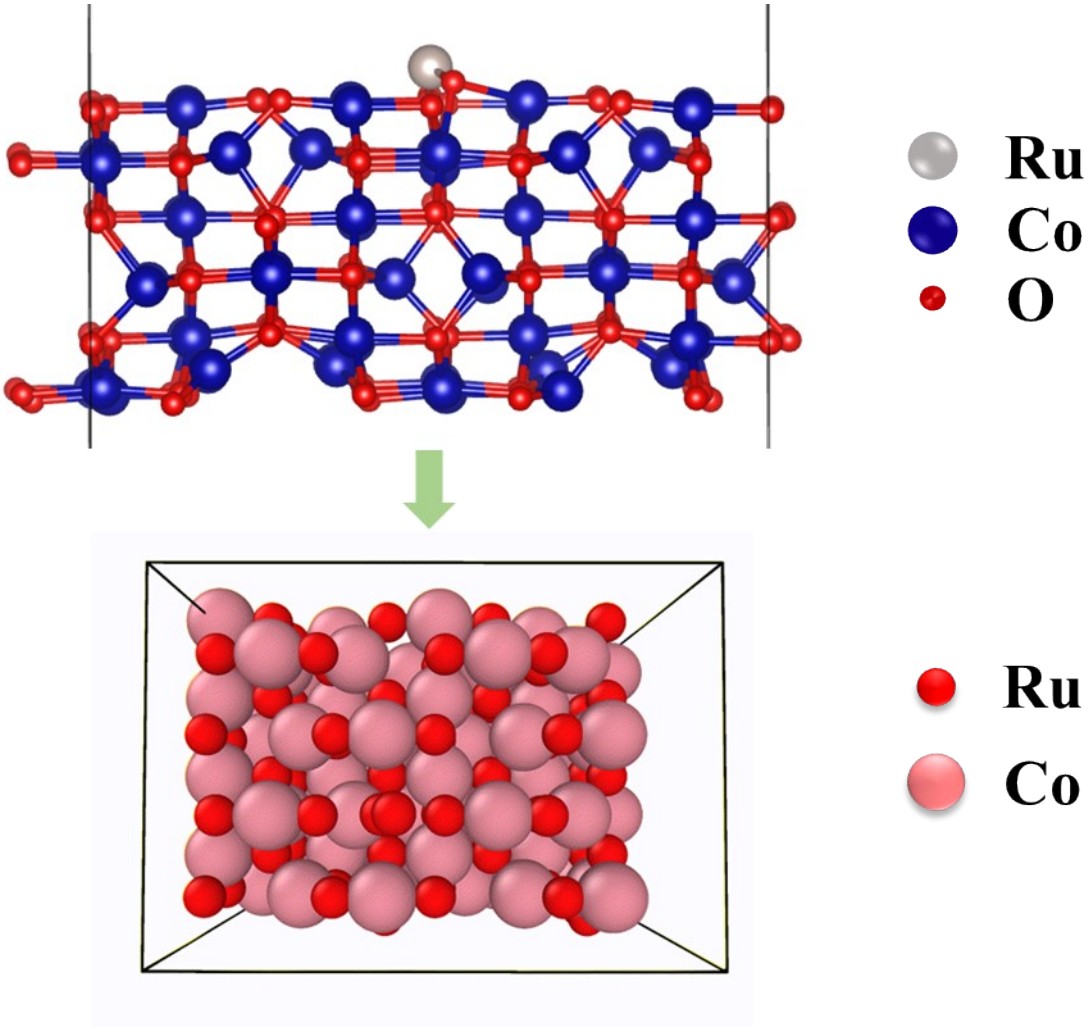

Figure S9. Gif is an optimization process, and Ru atoms are automatically migrated to the tetrahedron Co.

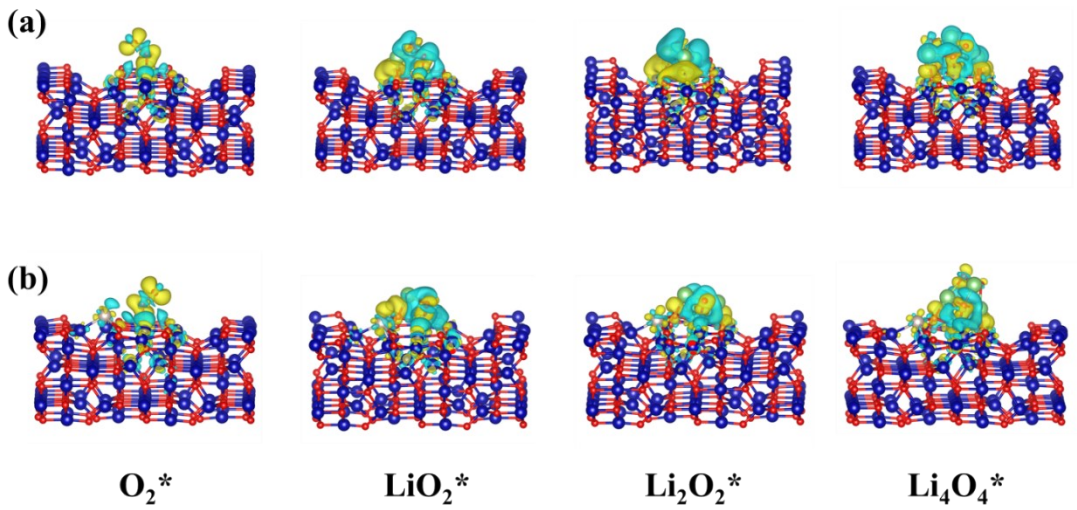

Figure S10. Electron localization function and charge density difference plots of different adsorbates (LiO_2*, Li_2O_2*, Li_4O_4*, and O_2*) on (a) Co_3O_4 and (b) Ru-Co_3O_4.

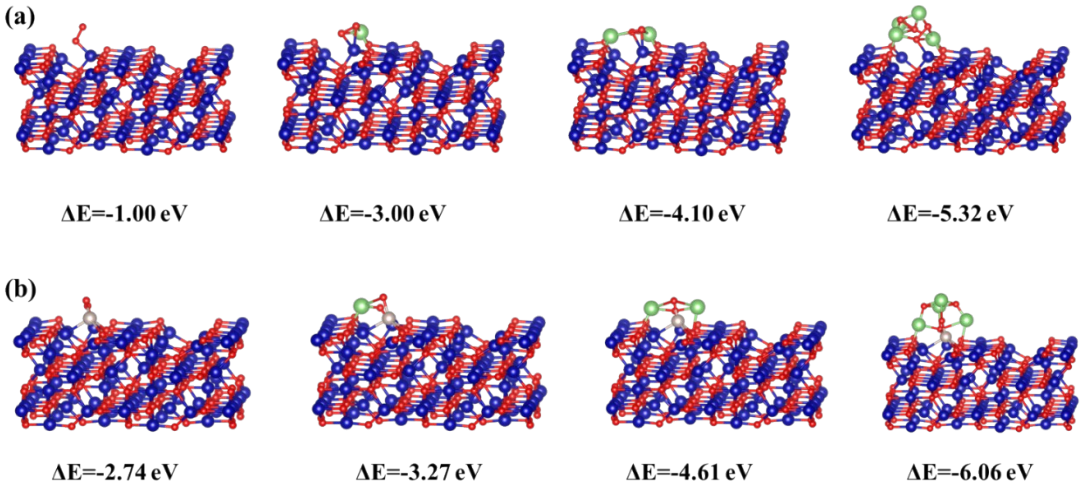

Figure S11. Binding energies and optimized structures of O_2, LiO_2, Li_2O_2 and $(Li_2O_2)_2$ at tetrahedral Co sites on the (a) Co_3O_4 and (b) Ru-Co_3O_4

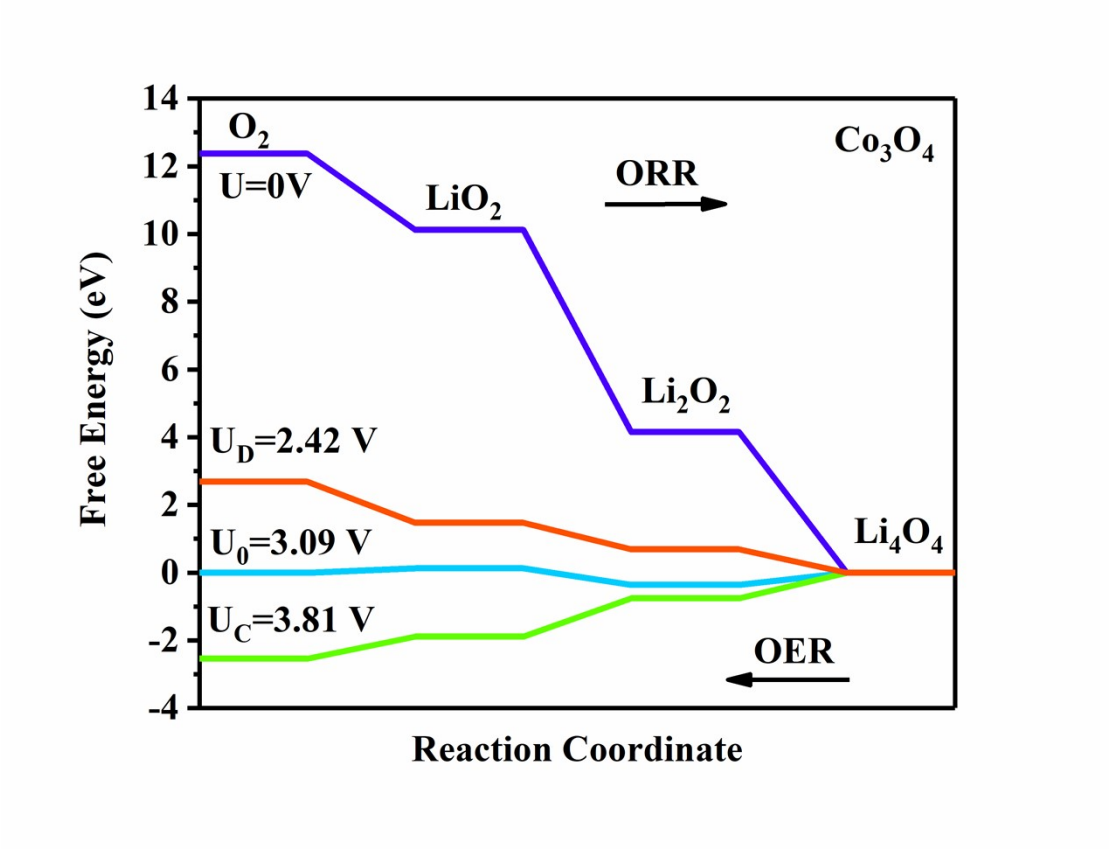

Figure S12. The free energy diagrams of ORR/OER process on Co_3O_4.

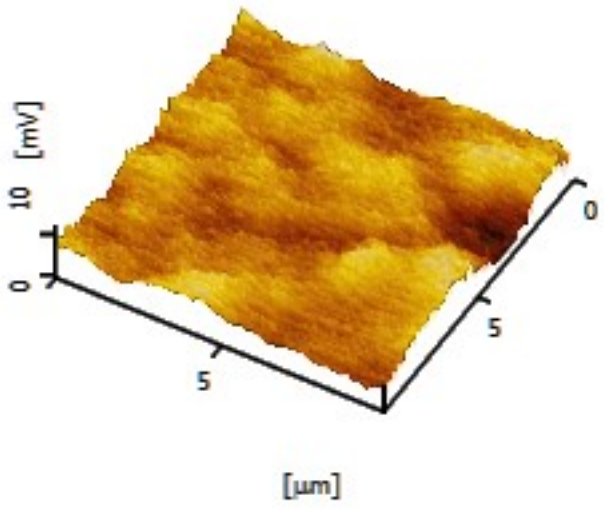

Figure S13. The surface work function of Ru-Co_3O_4.

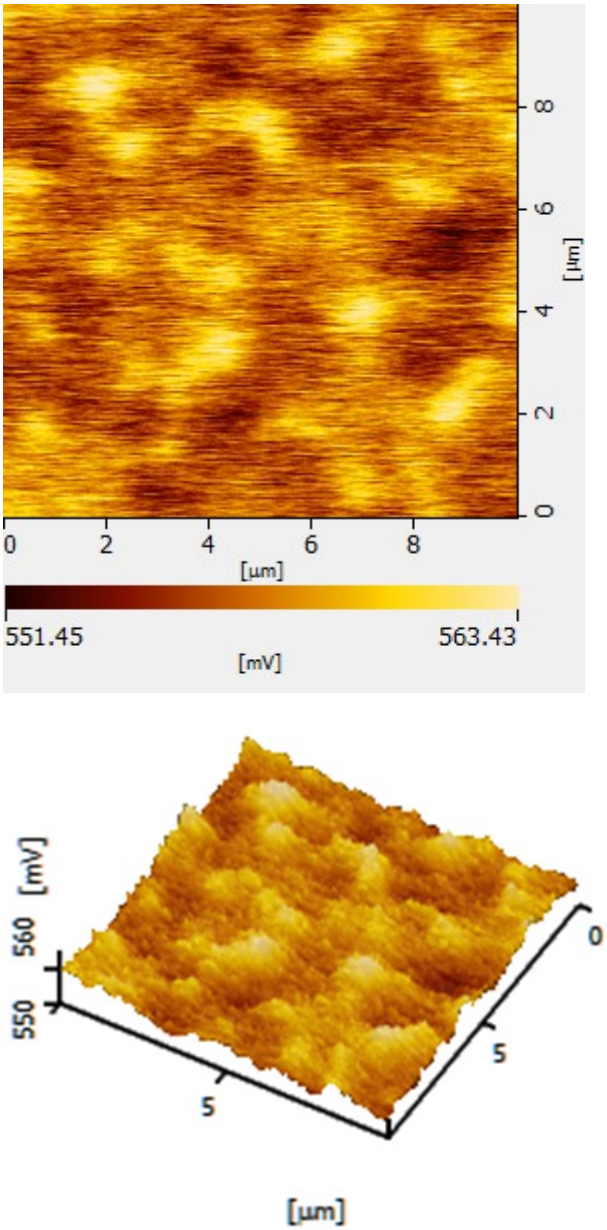

Figure S14. The surface work function of Co_3O_4.

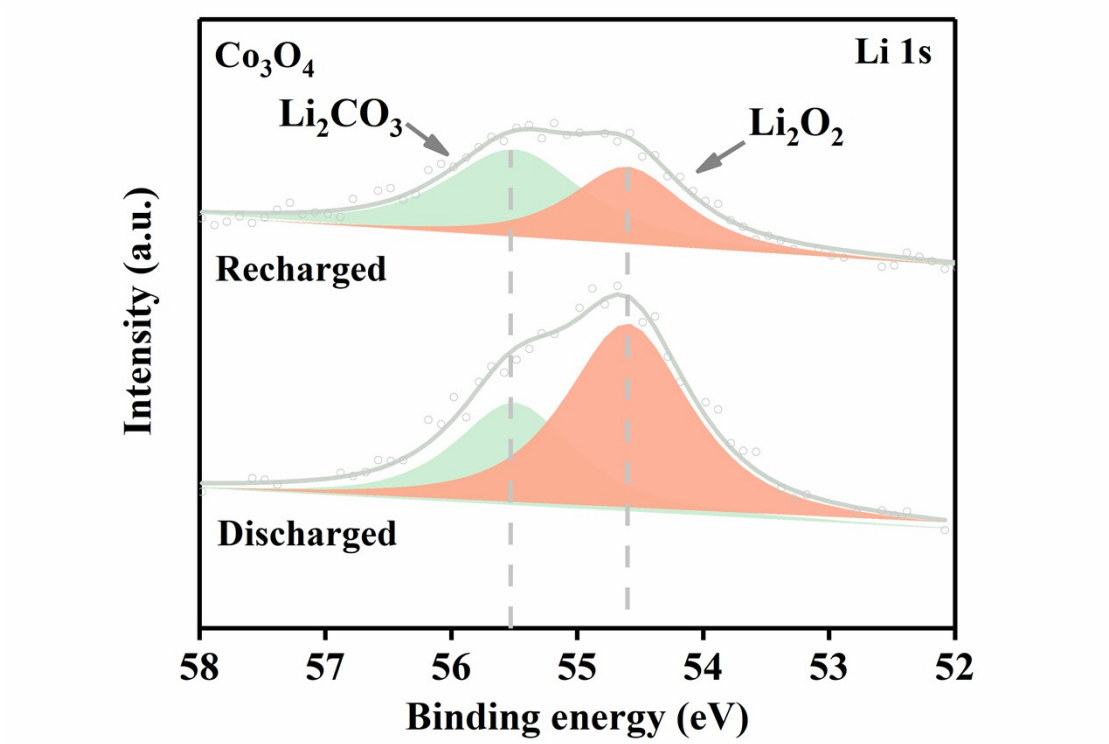

Figure S15. Li 1s XPS of Co_3O_4.

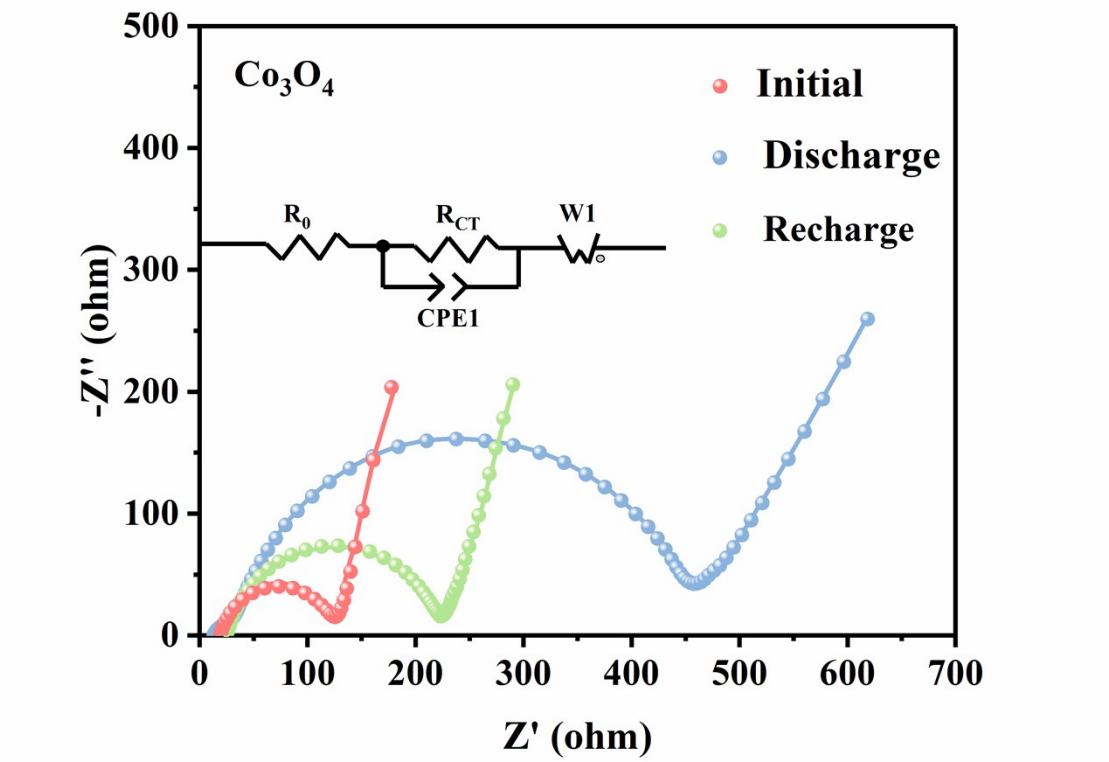

Figure S16. Nyquist plots of Co_3O_4 as cathode catalyst in LOBs at initial, 1st full discharge, and 1st full recharge.

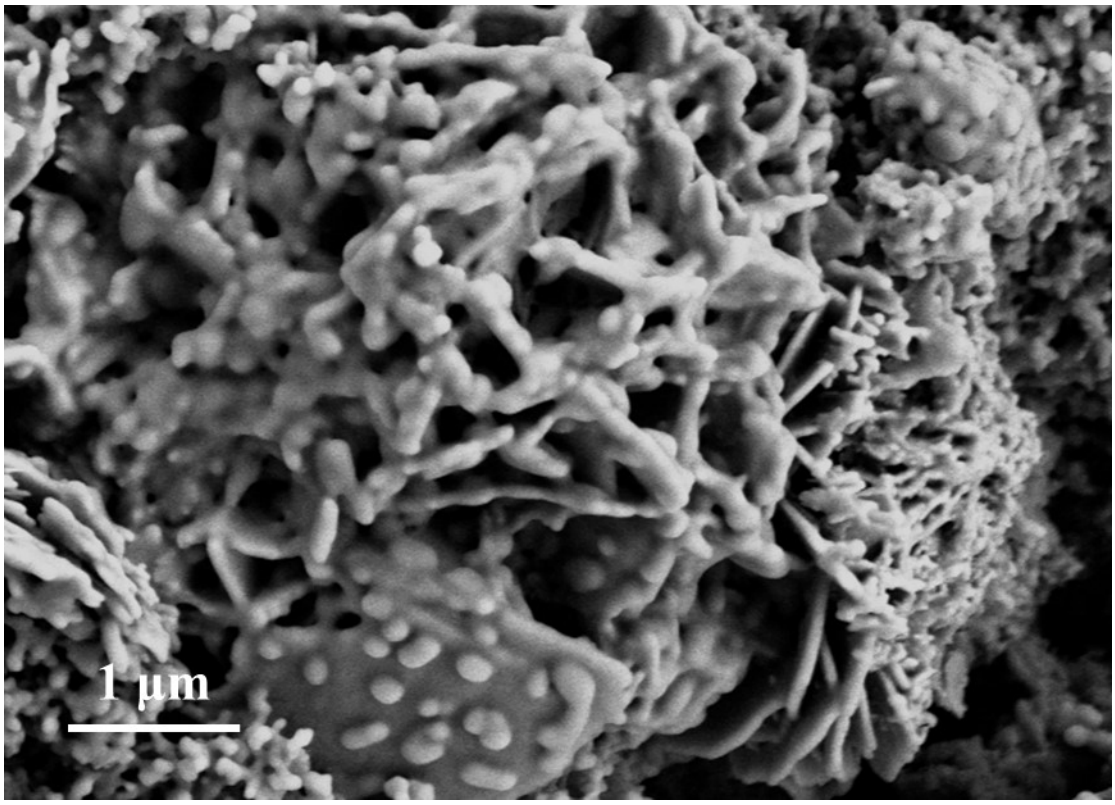

Figure S17. SEM image of Ru-Co_3O_4-based LOBs after charge-discharge cycles test.

Table S1. The comparison in catalytic performance between the Ru-Co_3O_4 battery and other batteries with different oxygen electrodes.

Catalyst	Electrolyte	Current density (mA/g)	Full discharge capacity (mAh/g)	Cycling conditions (current density and fixed capacity)	Cycle Number (cycles)	Reference
Ru-Co_3O_4	1 M LiTFSI in TEGDME	100	25000	300 mA/g 500 mAh/g	Over 500	This work
Ru-Co_3O_4	1 M LiTFSI in TEGDME	200	16861	200 mA/g 500 mAh/g	Over 180	Angewandte Chemie International Edition 62(15) (2023)
N-doped carbon sphere synthesized by MOF	1 M LiTFSI in TEGDME	500	18762	500 mA/g 1000 mAh/g	Over 200	International Journal of Energy Research 45(5) (2021) 7120-7128